Computational and Theoretical Chemistry 977 (2011) 62–68

Contents lists available at SciVerse ScienceDirect

Computational and Theoretical Chemistry

journal homepage: www.elsevier.com/locate/comptc

Theoretical study of CO adsorption and oxidation on the gold–palladium bimetal clusters

Song-Lin Peng [a], Li-Yong Gan [a,b], Ren-Yu Tian [a], Yu-Jun Zhao [a,b,*]

[a] Department of Physics, South China University of Technology, Guangzhou 510640, PR China
[b] State Key Laboratory of Luminescent Materials and Devices, South China University of Technology, Guangzhou 510640, PR China

ARTICLE INFO

Article history:
Received 29 July 2011
Received in revised form 25 August 2011
Accepted 10 September 2011
Available online 22 September 2011

Keywords:
Adsorption energy
Au/Pd bimetallic cluster
CO oxidation

ABSTRACT

Density functional theory (DFT) calculations are performed to investigate CO and O_2 adsorption as well as CO oxidation on the Au_mPd_n ($m + n = 2–6$) bimetallic clusters. It is found that the adsorption energies of both CO and O_2 on Au_mPd_n ($m + n = 2–6$) are greater than those on the pure gold clusters of corresponding sizes, and unexpectedly greater than those on Pd clusters in some cases. At the same time, the calculated reaction barrier of CO oxidation on Au_2Pd is lower than those on Au_3 and Pd_3, indicating that Au/Pd bimetallic cluster could potentially have a better catalytic activity for CO oxidation potentially.

1. Introduction

Gold(Au) is a noble metal and was considered to be catalytically inactive historically [1]. However, it has been changed since the report of gold nanoparticles on reducible oxide substrates exhibited great catalytic activity for CO oxidation even at very low temperature in 1987 [2]. It has also stimulated gold catalysis in a wide range of applications, such as hydrogenation of unsaturated hydrocarbons [3,4], CO oxidation [5–7], propylene epoxidation [8], water–gas shift [9–11] and selective oxidation [12], etc. The oxidation of CO is an important process for the environmental protection and safety concerning. Great efforts have been devoted to developing highly efficient catalysts to remove the poisonous CO gas from car exhaust [13,14] and hydrogen gases used for fuel cells in the last three decades [15]. Although the traditional transition metal catalysts, such as Pt, Pd, Rh, have been studied and used for a long time [16,17], there are still two challenging issues: one is the efficiency for CO oxidation at *low temperature*; and the other is the *affordable cost* for wide applications. Gold is regarded to be one of the promising catalysts to meet these challenges (The possibility of a relative low price for Au can not excluded though the price of gold soared up in the past years) [18].

Compared with the pure gold catalyst, bimetallic catalysts often exhibit enhanced catalytic stabilities, activities, or selectivities [19]. In recent years, Au/Pd bimetallic alloy catalysts have attracted special interest due to their unique activity and selectivity toward CO oxidation at low temperature [20–24]. Experiments have shown that the addition of a second metal into the pure Pd matrix can improve the activity of catalyst owing to the ligand effect [25] and ensemble effect [26,27]. The ligand effect refers to electronic modifications resulting from the additional metal, while the ensemble effect refers to the fact that the additional metal may block certain sites, reducing or eliminating the formation of an inhibiting species or an important intermediate. With the development of nanotechnology, many methods have been employed to obtain economical and efficient Au/Pd catalysts, including vapor and electrochemical deposition, and other techniques [28,29]. Compared with monometallic Au nanoparticles, Au/Pd bimetallic systems are often more attractive via the bi-functional mechanism [30]. Experimentally, Pd and Au are completely miscible as a solid solution because there is only about 4% lattice mismatch between Pd and Au. Goodman and co-workers [31] used physical vapor deposition on an Mo (1 1 0) substrate to obtain Pd, Au, Au/Pd mixtures and found that Au/Pd can highly promote acetoxylation of ethylene to vinyl acetate (VA) due to the ensemble effect [27]. Wu et al. [32] revealed that the activated barrier of CO oxidation on the AuPd (1 1 1) decreased compared with that on the pure Pd (1 1 1) due to the ligand effect through DFT calculations. For Au/Pd clusters, odd–even oscillations for the gaps between the highest occupied and the lowest unoccupied molecular-orbitals and the electron affinities have been observed in Au_nPd ($n = 1–4$) clusters [33]. Guczi et al. pointed out that both the size of Au/Pd clusters and substrates have great effect on CO oxidation on the AuPd/TiO_2 clusters [34]. However, the details of how the crucial factors of the Au/Pd catalysts, such as the structure, composition, and size,

* Corresponding author at: Department of Physics, South China University of Technology, Guangzhou 510640, PR China. Tel.: +86 020 87110426; fax: +86 020 87112837.
E-mail address: zhaoyj@scut.edu.cn (Y.-J. Zhao).

2210-271X/$ - see front matter © 2011 Elsevier B.V. All rights reserved.
doi:10.1016/j.comptc.2011.09.015

affect the activity of catalyst is still an open question. In particular, theoretical studies on the Au/Pd clusters are relative rare, in comparison to intensive studies on the Au/Pd surfaces.

In the present work, oxygen and carbon monoxide molecule adsorption on the Au_mPd_n $(m+n=2–6)$ clusters are studied in comparison with those on the corresponding pure Au and Pd clusters. The possible reaction pathways of CO oxidation on Au_2Pd are also studied and compared with those on the Au_3 and Pd_3 clusters.

2. Computational details

In this work, the density functional theory calculations were performed by the spin-polarized Kohn–Sham method with the DMOL^3 software package [35,36]. The generalized gradient approximation (GGA) with PW91 [37] formalism is employed for the exchange–correlation functional. We employed the double-numerical basis set with polarization functions (DNP) and a relativistic semi-core pseudopotential (DSPP) in the calculations.[35] All the calculations were based on Pulay's direct inversion of iterative subspace (DIIS) technique to accelerate SCF convergence. Fermi smearing was set to 0.005 Hartree during the electronic structure relaxation. Structure convergence was set to 1×10^{-5} a.u. for energies. As a test, the calculated distance of AuPd is 2.550 Å, in line with earlier theoretical value (2.560 Å) [38] and the experimental result (2.500 Å) [39] in literatures. The bond lengths of CO, O_2 in gas phase are calculated to be 1.141, 1.225 Å respectively, also in agreement with the available experimental data [39]. In addition, the calculated ionization potentials (IP) and electron affinities (EA) of the Au, Au_2, and Au_3 are also confirmed to be consistent with the experimental data (c.f. Table 1) [40–43].

The adsorption energy of CO and O_2 molecule are defined as:

$$E_{ad}(X) = E(Au/Pd) + E(X) - E(Au/Pd - X), \quad (1)$$

where the E(Au/Pd) is the energy of Au/Pd cluster, E(X) is the energy of adsorbate X in gas phase (X is CO or O_2), E(Au/Pd–X) is the total energy of X adsorbed Au/Pd cluster. Vibration frequency calculations are performed for all the optimized geometries, and those with one or more imaginary frequencies are discarded. The structure with the lowest energy is chosen as the ground-state geometry. The complete synchronous transit and quadratic synchronous transit (LST/QST) method is employed [44] to search the transition state and determine the activation barriers, and only the state with one imaginary frequency is considered as the transition state.

Table 1
Comparison of our calculated results and experimental data for CO, O_2 and Au_n $(n = 1–3)$ clusters, d is bond length in Å, f is vibration frequencies in cm^{-1}, VEA is vertical electron affinities, AIP is adiabatic ionization potentials. All energies are in eV.

	Cal.	Exp.
d_{C-O}	1.141	1.130[a]
f_{C-O}	2128.4	2143.0[a]
d_{O-O}	1.225	1.210[a]
f_{O-O}	1541.8	1580.0[a]
Au/VEA	1.90	2.25[d]
Au/AIP	9.65	9.23[b]
Au_2/VEA	1.61	2.01[e]
Au_2/AIP	9.32	9.16[c]
Au_3/VEA	2.03	3.77[d]
Au_3/AIP	7.27	7.27[c]

[a] Ref. [39].
[b] Ref. [42].
[c] Ref. [43].
[d] Ref. [40].
[e] Ref. [41].

3. Results and discussion

3.1. The structure of Au_mPd_n $(m+n=2–6)$

Fig. 1 depicts the lowest energy structure of the clusters of Au_n $(n = 2–6)$, Pd_n $(n = 2–6)$ and Au_mPd_n $(m+n=2–6)$. The optimized structures of the Au_n $(n = 3–6)$ are coplanar (generally ascribed to the relativistic effect [45]), in good agreement with the reported results in literatures [46,47], while the favorable structures of Pd_n $(n = 4–6)$ are demonstrated to be three-dimensional. The structures of Au_mPd_n $(m+n=2–6)$ are optimized from a large number of trial structures. The lowest energy structures obtained in this work are similar to those reported in Ref. [48] (except for Au_3Pd_2), in which the functional of B3LYP was employed. We also optimized Au_3Pd_2 with a trial structure as that in Ref. [48], and it was found to be converged to a high symmetry structure as shown in Fig. 1 with the total energy lowered by 0.3 eV. This discrepancy is expected to be ascribed to the different functionals adopted in the calculations. Meanwhile, we find that Au_mPd_n $(m+n=2–6)$ clusters are stabilized in three-dimensional structures when $n \geqslant \frac{2}{3}m$, while the other studied cases $(m+n=4–6)$ remain in

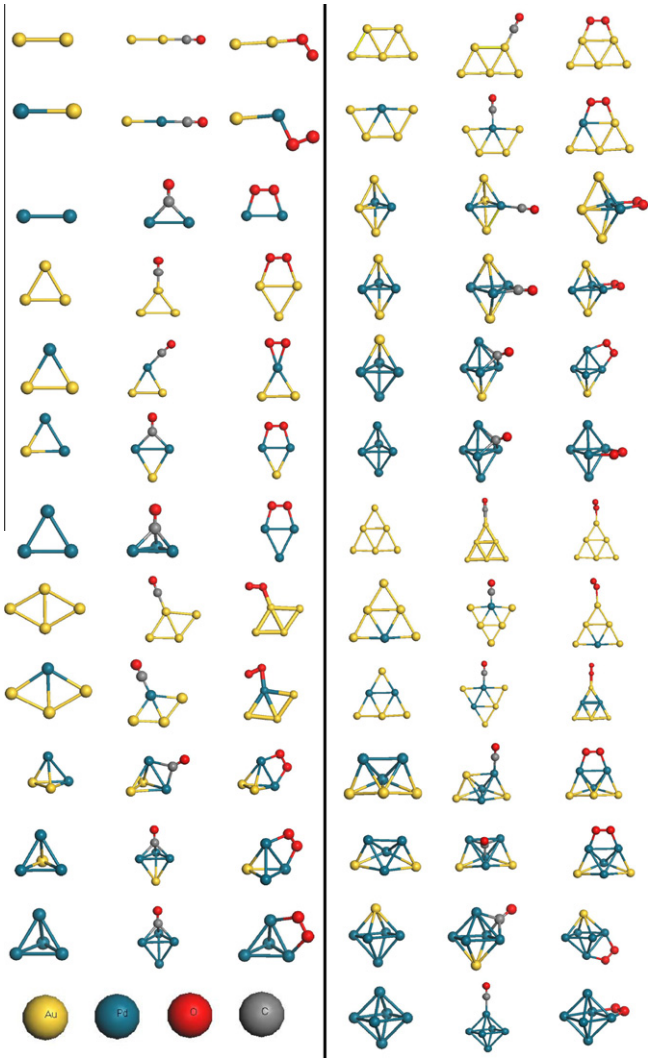

Fig. 1. The most stable structures of Au, Pd and Pd/Au clusters as well as their most stable CO and O_2 adsorption configurations. The yellow, blue, red and gray balls represent Au, Pd, O and C atoms, respectively. (For interpretation of the references to color in this figure legend, the reader is referred to the web version of this article.)

two-dimensional structures. Interestingly, our results also indicate that Pd atoms are preferred to connecting with each other to keep a maximum number of Pd–Pd bonds (c.f. Fig. 1) when Pd and Au form bimetallic clusters.

3.2. CO adsorption on Au, Pd, and Au/Pd clusters

The most stable configurations of CO adsorbed clusters are also shown in Fig. 1, and the detailed structural parameters, adsorption energies, and Mulliken net atomic charges are listed in Table 2. On the Au clusters, top sites are preferred with C atom directly connected to one of the Au atoms. The adsorption energies of CO are similar with each other on Au_2, Au_3, Au_4 (about 37 kcal/mol), and are reduced by ~10 kcal/mol on Au_5 and Au_6, though still clearly greater than that on pure Au (1 1 1), which is about 4.4 kcal/mol [49]. On the pure Pd clusters, CO prefers to adsorb at the bridge site of Pd_2 and hollow sites of Pd_3, Pd_4 and Pd_5, while top sites are the most stable ones on Pd_6. This is in line with the previous DFT studies [50,51]. Of note, CO prefers the bridge sites of (1 0 0) and three-fold hollow sites of (1 1 1) on Pd surfaces [52], while it prefers top sites of (1 0 0) and top sites of (1 1 1) on Au surfaces [49]. The adsorption energies of CO on Au/Pd bimetal clusters are greater than those on the Au clusters by about 1.8–28.1 kcal/mol. The preference of CO on Pd sites of Pd/Au clusters can be understood by the spatial distribution of the frontier molecular orbitals of bimetallic Au/Pd clusters, as shown in Fig. 2. Both the highest occupied molecular orbital (HOMO) and the lowest unoccupied molecular orbital (LUMO) of the bimetallic clusters are located on the Pd atoms, indicating the active centers.

The adsorption energies of CO on the Au, Au/Pd and Pd clusters are also illustrated in Fig. 3 for a clear comparison. It is understandable that the CO adsorption energies follow the sequence of Au < Au/Pd < Pd on clusters Au_mPd_n when $m + n \leqslant 4$. Unexpectedly, the CO adsorption energy on $AuPd_4$ is greater than that on Pd_4 and Pd_5, and the adsorption energy on Au_2Pd_4 is also greater than that on Pd_6. In fact, the local adsorption configurations for CO on Pd_4, Pd_5, and $AuPd_4$ are similar to each other, with CO normal to a plane of three Pd atoms above the center (c.f. Fig. 1). The unexpected stronger adsorption energy of CO on $AuPd_4$ is not easy to be explained by charge transfer and C–O bond length, since both values of $AuPd_4$ case are greater than those of Pd_4, but smaller that those of Pd_5 (c.f. Table 2).

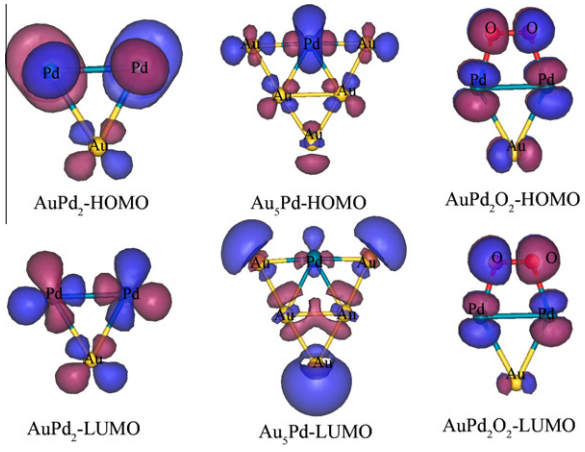

Fig. 2. The HOMO and LUMO isosurfaces for $AuPd_2$, Au_5Pd, and $AuPd_2O_2$.

The charges transferred from CO to cluster, q(CO), calculated by Mulliken analysis, are listed in Table 2. In many cases, stronger bindings between CO and clusters are corresponding to less q(CO). It is expected due to the well known charge donation and back donation mechanism in CO adsorption [53]. Compared with the free gas CO, the bond length of CO increased by 0.006–0.053 Å on all the studied clusters and the frequencies of CO decreased correspondingly.

3.3. O_2 adsorption on Au, Pd, and Au/Pd clusters

Subsequently, we take account of O_2 adsorption on the pure Au, pure Pd and Au/Pd clusters. The optimized structures of O_2 adsorbed clusters in their ground states are shown in Fig. 1. On the Au_2, Au_4, Au_6 clusters, top sites are the most favorable for O_2,

Table 2
The adsorption energies, bond lengths, frequencies, and Mulliken net atomic charges of CO and O_2 adsorbed on the Au, Pd and Au/Pd bimetallic clusters.

Cluster	CO				O_2			
	E_{ad} (kcal/mol)	d_{C-O} (Å)	f_{C-O} (cm^{-1})	q_{CO} (e)	E_{ad} (kcal/mol)	d_{O-O} (Å)	f_{O-O} (cm^{-1})	q_{O2} (e)
Au_2	37.4	1.148	2082.6	0.285	10.2	1.255	1328.0	−0.093
AuPd	39.2	1.154	2056.1	0.267	26.3	1.290	1208.7	−0.184
Pd_2	72.0	1.180	1861.1	0.183	43.8	1.370	899.0	−0.440
Au_3	37.8	1.152	2052.2	0.259	17.3	1.280	1220.0	−0.236
Au_2Pd	42.9	1.156	2034.0	0.228	22.4	1.301	1172.3	−0.247
$AuPd_2$	46.6	1.179	1852.3	0.189	36.9	1.324	1042.5	−0.296
Pd_3	62.7	1.200	1680.2	0.121	31.4	1.278	1237.3	−0.238
Au_4	37.6	1.149	2078.9	0.289	10.6	1.262	1290.8	−0.130
Au_3Pd	40.6	1.155	2030.7	0.257	26.8	1.300	1167.9	−0.323
Au_2Pd_2	41.3	1.175	1881.2	0.157	15.7	1.319	1047.2	−0.321
$AuPd_3$	46.8	1.197	1732.7	0.107	13.4	1.303	1125.8	−0.340
Pd_4	47.8	1.198	1692.5	0.103	24.0	1.217	1007.1	−0.310
Au_5	26.8	1.149	2077.5	0.271	20.8	1.348	993.3	−0.367
Au_4Pd	46.8	1.153	2060.7	0.307	28.6	1.341	996.8	−0.318
Au_3Pd_2	40.7	1.156	2011.3	0.240	27.7	1.317	1048.4	−0.270
Au_2Pd_3	33.9	1.179	1844.7	0.256	24.9	1.289	1170.5	−0.276
$AuPd_4$	53.3	1.200	1717.2	0.134	34.8	1.360	992.7	−0.385
Pd_5	46.4	1.203	1705.7	0.146	34.4	1.350	994.8	−0.350
Au_6	22.4	1.145	2095.3	0.265	5.3	1.252	1343.9	−0.101
Au_5Pd	37.4	1.153	2042.6	0.286	6.9	1.260	1340.3	−0.124
Au_4Pd_2	22.8	1.152	2051.1	0.305	34.8	1.350	997.2	−0.386
Au_3Pd_3	25.1	1.157	2018.1	0.249	41.5	1.360	992.5	−0.401
Au_2Pd_4	50.5	1.200	1721.4	0.156	34.4	1.330	998.7	−0.341
$AuPd_5$	44.7	1.190	1750.5	0.160	37.1	1.350	998.0	−0.350
Pd_6	40.4	1.160	2027.2	0.254	35.7	1.300	999.1	−0.349

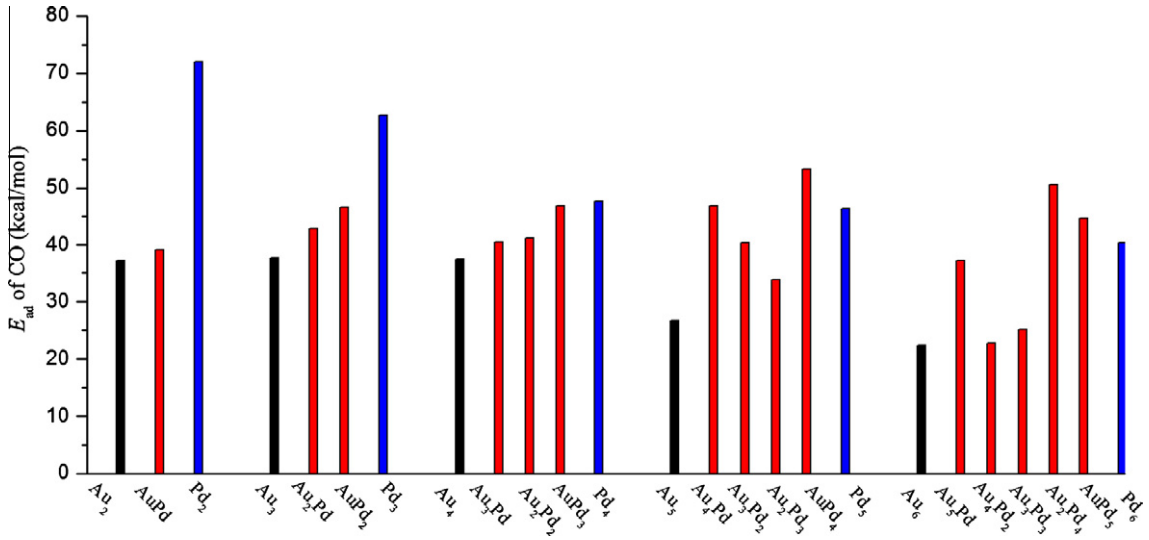

Fig. 3. A comparison of adsorption energies of CO on the Au, Au/Pd and Pd clusters. Black, red, and blue bars are corresponding to Au, Au/Pd, and Pd, respectively. (For interpretation of the references to color in this figure legend, the reader is referred to the web version of this article.)

while on the Au_3 and Au_5, O_2 prefers at the bridge sties. The adsorption energies of O_2 on the Au_n (n = 2–6) are 10.2, 17.3, 10.6, 20.8, 5.3 kcal/mol, displaying a clear odd–even oscillation with a stronger bonding on the odd number clusters. This is ascribed to the unpaired electron in the Au clusters with odd numbers [53]. The adsorption energies of O_2 on the pure Au clusters are in good agreement with the earlier calculations [54,55]. Yet on the Pd clusters, bridge sites are the most stable sites for O_2 adsorption, with two oxygen atoms directly bonded to Pd atoms. The adsorption of O_2 on the Pd_n (n = 2–6) are clearly stronger than the Au clusters.

On the Au/Pd bimetallic clusters, O_2, prefers top sites on the AuPd, Au_2Pd, Au_3Pd, Au_5Pd and Au_4Pd_2 clusters, while it prefers bridge sites on the rest of Au/Pd clusters (c.f. Fig. 1). Again, Pd atoms are the most active sites according to the earlier HOMO/LUMO analysis (c.f. Fig. 2). The O_2 adsorption energies on the Au/Pd clusters are listed in Table 2. In order to compare its bonding strength on the Au, Au/Pd and Pd clusters, the adsorption energies of O_2 are also illustrated in Fig. 4. We can see that for a given size of clusters with $m + n$ = 3–6, the greatest adsorption energy of O_2 exists in Au/Pd clusters, not in pure Au or Pd clusters. For instance, the O_2 adsorption energies on the $AuPd_4$ is 34.8 kcal/mol, which is the largest among the Au_mPd_n of size $m + n$ = 5. When the O_2 is bonded on the $AuPd_4$, the O–O bond length is elongated to 1.360 Å from the initial 1.225 Å and the corresponding O_2 vibration frequency shifts from 1541.8 cm^{-1} of free O_2 to 992.7 cm^{-1}.

3.4. CO oxidation on Au, Au/Pd and Pd clusters

In order to compare CO oxidation on Au, Pd and Au/Pd bimetallic clusters, we have investigated possible reaction paths on prototype clusters of Au_3, Pd_3, and Au_2Pd. Two different pathways for CO oxidation are considered here in analogy to the pathways discussed in earlier literature [56]. One involves CO attacking the initial complexes of Au_3–O_2, Pd_3–O_2 and Au_2Pd–O_2 (denoted as path-1), while the other is that the production of CO_2 followed by the interaction of free CO with the O_2 and CO adsorbed Au_3, Pd_3 and Au_2Pd (denoted as path-2).

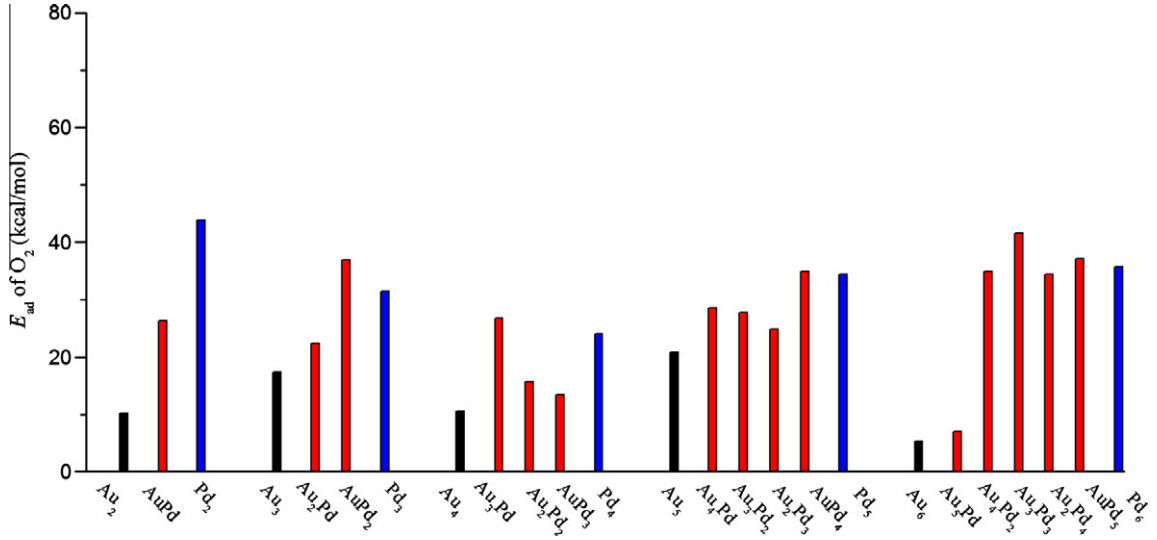

Fig. 4. A comparison of adsorption energies of O_2 on the Au, Au/Pd and Pd clusters. Black, red, and blue bars are corresponding to Au, Au/Pd, and Pd, respectively. (For interpretation of the references to color in this figure legend, the reader is referred to the web version of this article.)

3.4.1. CO oxidation on Au_3

The calculated potential energy surface of path-1 is shown in Fig. 5. Along path-1, CO is assumed to bind to the O_2 pre-adsorbed Au_3 to form an intermediate state, denoted as IM1 in Fig. 5. This structure is energetically favored by 20.6 kcal/mol than that of the non-interacted reactants, free CO and Au_3–O_2. The transition state of path-1, denoted as TS-1, is 17.0 kcal/mol higher than IM1. The O–O bond length in TS-1 is elongated to 1.370 Å from 1.280 Å in the initial Au_3–O_2 state and 1.283 Å in IM1 state. While the O–O bond breaks, a new C–O bond is formed. TS-1 has only one imaginary frequency, which is $-518.9\ cm^{-1}$. Then, the product-like intermediate state IM2 is formed following TS-1. The relative high barrier in Path1 implies that CO oxidation is hardly following this pathway in reality. Our calculated results are in agreement with the earlier theoretic calculations [55].

As for path-2, the free gas CO is assumed to approach the O_2 in the O_2 and CO pre-adsorbed Au_3 cluster. The reaction starts with the formation of IM3, an intermediate state of free CO coupled with Au_3–CO–O_2 complex, which is energetically favored by 58.3 kcal/mol than the free reactants, CO and Au_3. The reaction involves the transition state TS-2, where the O–O bond length is changed to 1.347 Å from 1.283 Å in IM3. In TS-2, C atom of the free CO is just 1.670 Å away from an O atom of O_2 molecule, indicating that a new C–O bond forms. The only imaginary frequency in the TS-2 is $-515.0\ cm^{-1}$. The barrier along this pathway is 13.4 kcal/mol, which is lower than that of the path-1, demonstrating that the pre-adsorption CO can prompt CO oxidation. The promotion may result from the charge transfers from CO to the cluster. On the CO adsorbed Au_3, there are 0.259 *e* charges donated from CO to Au_3, possibly leading more charges transferred from cluster to the anti-bonding π^* orbital of O_2 to activate O_2.

3.4.2. CO oxidation on Pd_3

In order to further compare the activity of Au/Pd bimetallic catalyst with Pd cluster for CO oxidation, CO oxidation on Pd_3 is also investigated. The reaction is also studied along two paths, Pd_3-path-1 and Pd_3-path-2.

Along the Pd_3-path-1, O_2 is adsorbed on the Pd_3 cluster, denoted as IM5 in Fig. 6. Then, CO reacts with the pre-adsorbed O_2. IM5 is energetically favored by 30.3 kcal/mol than the separated reactants, free CO and Pd_3–O_2. In the reaction of IM5 to its transition state, TS-3 (the imaginary frequency is $-329.2\ cm^{-1}$), the O–O bond length increases from 1.335 Å to 2.111 Å. In IM6, a new C–O bond is formed as the O–O bond is broken. The calculated reaction barrier of this reaction path is 40.4 kcal/mol. The high barrier is mainly due to the strong bonding of O_2 on the bridge site of two Pd atoms in IM5, where the O–Pd bond is difficult to break.

On the second pathway, the reaction starts with the formation of IM7, which is more stable than the separated reactants by 47.2 kcal/mol. The transition state is denoted as TS-4 (the imaginary frequency is $-410.4\ cm^{-1}$) in Fig. 6. In TS-4, the O–O bond length increases by 0.23 Å, from 1.279 Å in IM7. In IM8, the O–O bond is broken and new C–O bond is formed. Compared with the reaction barrier of Pd_3-path-1, the reaction barrier of Pd_3-path-2 is also lowered by 2.4 kcal/mol.

3.4.3. CO oxidation on Au_2Pd

We select Au_2Pd as the simplest Au/Pd bimetallic cluster to explore the CO oxidation on the bimetallic clusters with respect to CO oxidation on Au_3 and Pd_3 clusters. The CO oxidation on Au_2Pd is also investigated with the two paths similar to those discussed in Section 3.4.1. The potential energy surface profiles (PES) for Au_2Pd are shown in Fig. 7.

In the case of Au_2Pd-path-1, CO reacts with the pre-adsorbed O_2. The reaction starts from IM9, which is more stable than the two individual reactants by 13.0 kcal/mol. This intermediate state is converted to IM10 via the TS-5 with a barrier of 2.7 kcal/mol. In TS-5 (the imaginary frequency is $-247.5\ cm^{-1}$), the O_2 molecule is being activated as the O–O bond length is elongated to 1.291 Å from 1.275 Å in the initial state, and the O–C distance is shortened to 2.412 Å from 3.180 Å in IM9.

In path-2 of Au_2Pd, two CO molecules are involved in the CO oxidation. The reaction proceeds with two steps. The first is that CO binds on the Au atom with O_2 pre-adsorbed on the Pd atom, followed by a reaction of a free CO with the adsorbed O_2 molecules. The second step involves the breaking of O–O bond and the formation of a new C–O bond. With the aid of CO molecule, the reactions from the intermediate IM11 state, to the product-like, IM12, via a transition state of TS-6. The imaginary frequency of TS-6 is $-110.4\ cm^{-1}$. Compared to IM4 in Fig. 5, the intermediate IM12

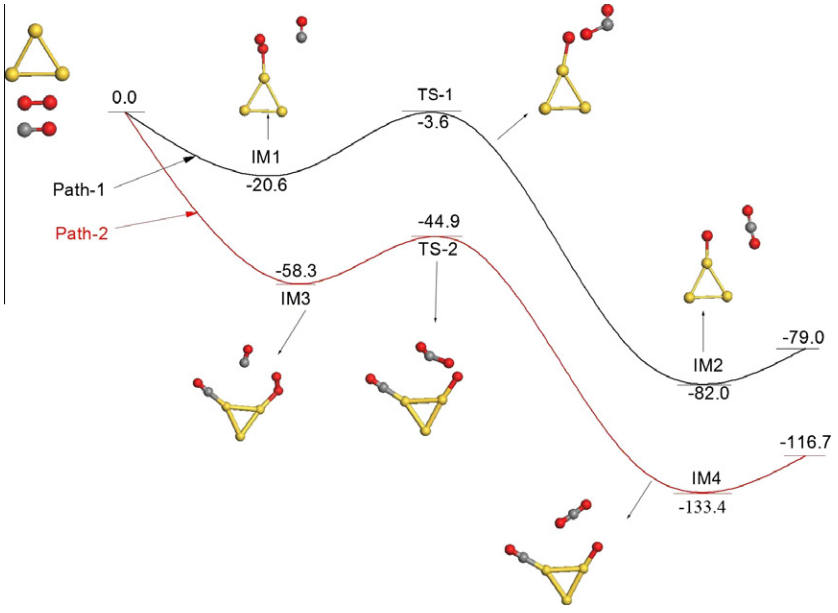

Fig. 5. Potential energy surfaces for CO oxidation on Au_3 cluster along path-1 (black line) and path-2 (red line). The corresponding intermediates and transition states related to the two pathways are also presented. The sum of energies of free Au_3, O_2 and CO is set to zero as a reference. All the energies are in kcal/mol. The yellow, gray, and red balls denote Au, C, and O atoms, respectively. (For interpretation of the references to color in this figure legend, the reader is referred to the web version of this article.)

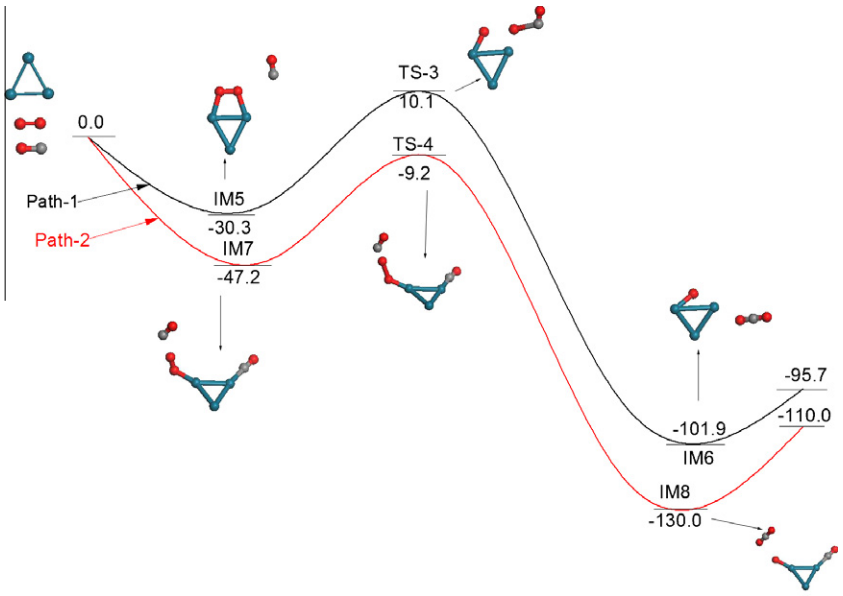

Fig. 6. Potential energy surfaces for CO oxidation on Pd_3 cluster along path-1 (black line) and path-2 (red line). The corresponding intermediates and transition states related to the two pathways are also presented. The sum of energies of free Pd_3, O_2 and CO is set to zero as a reference. All the energies are in kcal/mol. The blue, gray, and red balls denote Pd, C and O atoms, respectively. (For interpretation of the references to color in this figure legend, the reader is referred to the web version of this article.)

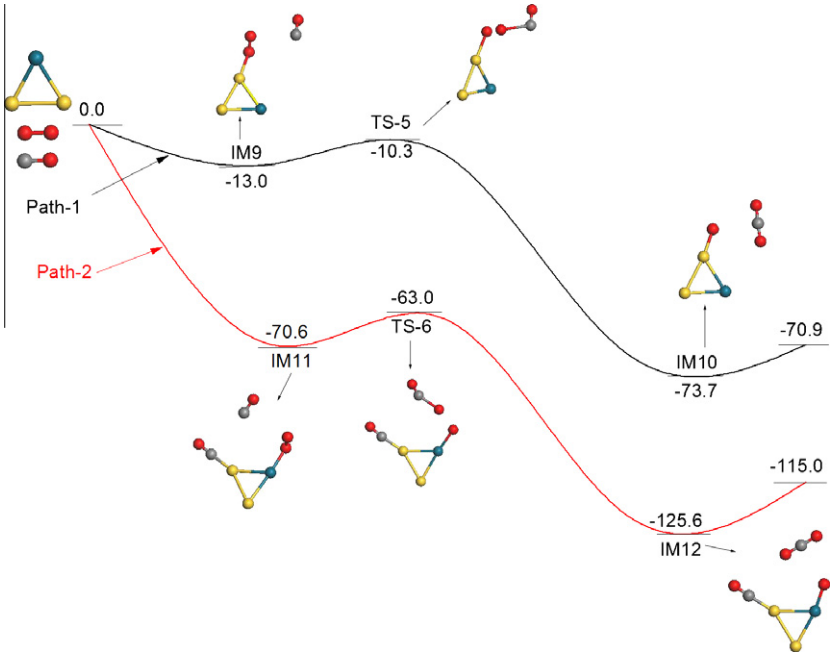

Fig. 7. Potential energy surfaces for CO oxidation on Au_2Pd cluster along path-1 (black line) and path-2 (red line). The corresponding intermediates and transition states related to the two pathways are also presented. The sum of energies of free Au_2Pd, O_2 and CO is set to zero as a reference. All the energies are in kcal/mol. The yellow, blue, gray, and red balls denote Au, Pd C, and O atoms, respectively. (For interpretation of the references to color in this figure legend, the reader is referred to the web version of this article.)

is less stable. This is due to the Au_3 cluster has an odd number of electrons, while Au_2Pd has an even number of electrons. Consequently, the O adsorption energy on Au_3 (3.33 eV) is greater than that on Au_2Pd (3.03 eV). The calculated barrier of this reaction is 7.6 kcal/mol. In CO oxidation, the activation of O_2 is often regarded as the rate-determining step. The lower calculated barrier energy of the CO oxidation on Au_2Pd indicates that CO could be efficiently oxidized at low temperature on the Au/Pd clusters.

From the above discussion, it is clear that the reaction barrier on the Au_2Pd is lower than those on the Au_3 and Pd_3 clusters, independent of reaction paths of CO oxidation studied. It is demonstrated that the reactivity of the Au/Pd bimetallic cluster for CO oxidation could be higher than that of pure Au and Pd clusters, indicating the efficiency of Au/Pd alloys at low temperature.

4. Conclusions

In this paper, we have studied the most stable structures of Au_mPd_n ($m + n = 2$–6) clusters, as well as O_2 and CO adsorption

on these clusters. We find that Au_mPd_n clusters are stabilized in three-dimensional structures when $n \geqslant \frac{2}{3}m$ in the studied cases, while other clusters keep in two-dimensional structures as for the small Au clusters. Interestingly, CO and O_2 could be more stable on Au/Pd clusters than Au and Pd clusters with corresponding size. At the same time, CO oxidation barrier on Au_2Pd is found to be lower than that on Au_3 and Pd_3, indicating that Au/Pd bimetallic clusters could have higher reactivity for CO oxidation.

Acknowledgments

This work is supported by MOST under project 2010CB631302, and the Fundamental Funds for the Central Universities, SCUT, under projects 2009ZZ0068, 2009ZM0165, and 2011ZG0017, and completed with the cooperation of HPC Lab, Shenzhen Institute of Advanced Technology, CAS, China.

References

[1] B. Hammer, J.K. Norskov, Nature 376 (1995) 238–240.
[2] M. Haruta, T. Kobayashi, H. Sano, N. Yamada, Chem. Lett. 2 (1987) 405–408.
[3] M. Haruta, Catal. Today 36 (1997) 153–166.
[4] M. Haruta, M. Date, Appl. Catal., A Gen. 222 (2001) 427–437.
[5] F. Boccuzzi, A. Chiorino, M. Manzoli, P. Lu, T. Akita, S. Ichikawa, M. Haruta, J. Catal. 202 (2001) 256–267.
[6] W. An, Y. Pei, X.C. Zeng, Nano Lett. 8 (2008) 195–202.
[7] G.C. Bond, D.T. Thompson, Catal. Rev. Sci. Eng. 41 (1999) 319–388.
[8] R.J. Davis, Science 301 (2003) 926–927.
[9] D. Andreeva, V. Idakiev, T. Tabakova, L. Ilieva, P. Falaras, A. Bourlinos, A. Travlos, Catal. Today 72 (2002) 51–57.
[10] F. Boccuzzi, A. Chiorino, M. Manzoli, D. Andreeva, T. Tabakova, J. Catal. 188 (1999) 176–185.
[11] Q. Fu, H. Saltsburg, M. Flytzani-Stephanopoulos, Science 301 (2003) 935–938.
[12] R.J.H. Grisel, B.E. Nieuwenhuys, J. Catal. 199 (2001) 48–59.
[13] G.C. Bond, D.T. Thompson, Gold Bull. 33 (2000) 41–51.
[14] A.S.K. Hashmi, G.J. Hutchings, Angew. Chem. Int. Ed. 45 (2006) 7896–7936.
[15] M. Valden, X. Lai, D.W. Goodman, Science 281 (1998) 1647–1650.
[16] D.I. Enache, J.K. Edwards, P. Landon, B. Solsona-Espriu, A.F. Carley, A.A. Herzing, M. Watanabe, C.J. Kiely, D.W. Knight, G.J. Hutchings, Science 311 (2006) 362–365.
[17] T. Bunluesin, R.J. Gorte, G.W. Graham, Appl. Catal., B-Environ. 15 (1998) 107–114.
[18] C.W. Corti, R.J. Holliday, D.T. Thompson, Appl. Catal., A Gen. 291 (2005) 253–261.
[19] K.M. Neyman, F. Illas, Catal. Today 105 (2005) 2–16.
[20] X.H. Hao, B. Shan, J. Hyun, N. Kapur, K. Fujdala, T. Truex, K. Cho, Top. Catal. 52 (2009) 1946–1950.
[21] K. Persson, A. Ersson, K. Jansson, N. Iverlund, S. Jaras, J. Catal. 231 (2005) 139–150.
[22] K.V. Rybalka, M.R. Tarasevich, B.M. Grafov, V.A. Bogdanovskaya, L.A. Beketaeva, E.N. Loubnin, Y.A. Kolbanovskii, J. New Mater. Electrochem. Syst. 10 (2007) 81–89.
[23] T.J. Schmidt, Z. Jusys, H.A. Gasteiger, R.J. Behm, U. Endruschat, H. Boennemann, J. Electroanal. Chem. 501 (2001) 132–140.
[24] J.B. Xu, T.S. Zhao, S.Y. Shen, Y.S. Li, Int. J. Hydrogen Energy 35 (2010) 6490–6500.
[25] P. Liu, J.K. Norskov, Phys. Chem. Chem. Phys. 3 (2001) 3814–3818.
[26] F. Maroun, F. Ozanam, O.M. Magnussen, R.J. Behm, Science 293 (2001) 1811–1814.
[27] M.S. Chen, D. Kumar, C.W. Yi, D.W. Goodman, Science 310 (2005) 291–293.
[28] S.Y. Jo, B.R. Kang, J.T. Kim, H.W. Ra, Y.H. Im, Nanotechnology 21 (2010) 055604–055609.
[29] A. Damian, F. Maroun, P. Allongue, Phys. Rev. Lett. 102 (2009) 196101–196105.
[30] M. Watanabe, J. Electroanal. Chem. 60 (1975) 112–119.
[31] C.W. Yi, K. Luo, T. Wei, D.W. Goodman, J. Phys. Chem. B 109 (2005) 18535–18540.
[32] J. Zhang, H.M. Jin, M.B. Sullivan, F. Chiang, H. Lim, P. Wu, Phys. Chem. Chem. Phys. 11 (2009) 1441–1446.
[33] B.R. Sahu, G. Maofa, L. Kleinman, Phys. Rev. B 67 (2003) 115420–115425.
[34] L. Guczi, A. Beck, A. Horvath, Z. Koppany, G. Stefler, K. Frey, I. Sajo, O. Geszti, D. Bazin, J. Lynch, J. Mol. Catal., A-Chem. 204 (2003) 545–552.
[35] B. Delley, J. Chem. Phys. 92 (1990) 508–513.
[36] B. Delley, J. Chem. Phys. 113 (2000) 7756–7764.
[37] J.P. Perdew, Y. Wang, Phys. Rev. B 45 (1992) 13244–13249.
[38] V. Agacino, Int. J. Quantum Chem. 108 (2008) 1796–1801.
[39] C.D.R. Lide, Handbook of Chemistry and Physics, CRC Press, Boca Raton, FL, 1995.
[40] K.J. Taylor, H.C. Pettiette, J. Chem. Phys. 96 (1992) 3319–3329.
[41] J. Ho, K. Ervin, W. Lingerger, J. Chem. Phys. 93 (1990) 6987–7002.
[42] C.E. Moore, Atomic Energy Levels. Ed. Washington, DC, 1958.
[43] M.A. Cheeseman, J.R. Eyler, J. Phys. Chem. 96 (1992) 1082–1087.
[44] W.N. Lipscomb, T.A. Halgren, Chem. Phys. Lett. 49 (1977) 225–232.
[45] P. Pyykko, Angew. Chem. Int. Ed. 43 (2004) 4412–4456.
[46] A. Deka, R.C. Deka, J. Mol. Struct.-Theochem. 870 (2008) 83–93.
[47] P. Jensen, R. Mod. Phys. 71 (1999) 1695–1735.
[48] G. Zanti, D. Peeters, J. Phys. Chem. A 114 (2010) 10345–10356.
[49] L.Y. Gan, Y.-J. Zhao, J. Chem. Phys. 133 (2010) 094703–094710.
[50] N.S. Phala, G. Klatt, E. van Steen, Chem. Phys. Lett. 395 (2004) 33–37.
[51] B. Kalita, R.C. Deka, Eur. Phys. J. D 53 (2009) 51–58.
[52] C.J. Zhang, P. Hu, J. Am. Chem. Soc. 123 (2001) 1166–1172.
[53] G. Blyholder, J. Phys. Chem. 68 (1964) 2772–2778.
[54] X.L. Ding, Z.Y. Li, J.L. Yang, J.G. Hou, Q.S. Zhu, J. Chem. Phys. 120 (2004) 9594–9600.
[55] R. Coquet, K.L. Howard, D.J. Willock, Chem. Soc. Rev. 37 (2008) 2046–2076.
[56] F. Wang, D.J. Zhang, X.H. Xu, Y. Ding, J. Phys. Chem. C 113 (2009) 18032–18039.